The Pentacovalent Phosphorus Intermediate of a Phosphoryl Transfer Reaction

Materials and Methods

The *Lactococcus lactis* β-PGM (*1, 2*) clones were expressed in *E. coli* and purified as described (*3*) for both wild-type and selenomethionine (SeMet) substituted proteins. Protein was resuspended in 1mM K$^+$HEPES buffer (pH 7.5) plus 10 mM MgCl$_2$ and 1 mM dithiothreitol and crystals were grown from 0.1 M ammonium fluoride and 16% w/v PEG 3350 (final drop pH measured as 6.9) at 18˚C using the vapor-diffusion method with hanging-drop geometry, as previously described (*3*). Both wild type and SeMet-substituted proteins were co-crystallized in the presence of 5 mM substrate (either G1P or G6P) and flash frozen in liquid nitrogen, using Paratone-N (Hampton Research) as cryoprotectant. Single-wavelength datasets for wild-type β-PGM crystals, cocrystallized with either G1P or G6P, were collected at -180˚C on beamline 14-BMC, Argonne National Laboratories using a ADSC Quantum4 detector. The multi-wavelength anomalous diffraction data for SeMet β-PGM cocrystallized with G6P were collected to 1.7 Å resolution on beamline X4A at Brookhaven National Laboratories using a ADSC Quantum4 detector. MAD data were collected at -180˚C at three wavelengths with a single pass of 180˚. The DENZO and SCALEPACK programs (*4*) were used for data indexing, reduction, and scaling. Initial attempts to solve the phases of the substrate soaked β-PGM via the molecular replacement method using the unliganded β -PGM structure ((*3*), PDB accession code 1LVH) as the search model were unsuccessful, resulting in a structure with good electron density of the core domain for the protein and poor electron density for the cap domain. This failure was, in retrospect; probably due to

the fact that moving the two domains of the protein as rigid bodies did not make an adequate model of the "closed" enzyme conformer. The structure of SeMet substituted β-PGM co-crystallized with G6P was therefore solved *de novo* using MAD phase determination. Initial phases were obtained using SOLVE version 2.1 (*5*) yielding a clear electron density for the polypeptide chain with distinct solvent boundaries. The map was improved further using solvent flattening in the program RESOLVE version 1.9 (*6*). Model building and refinement were performed with the molecular graphics program O (*7*) and the program CNS (*8*) using simulated annealing with torsional dynamics performed against a Maximum Likelihood Hendrickson-Lattman target. The electron density from a F_o-F_c map depicted a clear density for a β-G1,6-P intermediate and the Mg(II) cofactor in the active site. Water molecules were added to the model after R_{free} values below 30 were obtained, followed by the model for β-G1,6-P. There was no ambiguity in the placement of the liganded molecules in either subunit, because of the strong electron density of the Mg^{2+} (>14σ) and PO_4^{3-} (>13σ) in the sigmaa weighted $2F_o$-F_c map (*9*).

Report

The overall structure of β-PGM is similar to other two-domain protein members of the haloalkanoic dehalogenase superfamily (*10-13*). Comparison of the β-G1,6-P intermediate complex presented here with that of the previously determined phosphorylated enzyme-Mg(II) complex (*3*) shows that any *intradomain* conformational changes are not large since the two domains that comprise the enzyme superimpose with a low rmsd of 0.88Å (cap) and 0.77Å (core) for Cα atoms (see Figure S1).

The connectivity of the density corresponding to the pentavalent oxyphosphorane comprised of the enzyme Asp8 OD1 and the β-G1,6-P intermediate is most clearly demonstrated by the electron density map (see Figure S2a) calculated with data to 2.0Å resolution (where the resolution of the data is equal to the apical bond lengths). It should be noted that the same structure is observed for the data set collected from crystals grown in the presence of G1P and from crystals grown in the presence of G6P. Thus, the observed intermediate is a true intermediate and not the result of non-productive complex formation. In addition, the interpretation that the phosphorus density observed does not represent an average of the structures of the phosphorylated Asp and the phosphorylated C1(O) species is supported by calculating the difference electron density due to the anomalous signal from the phosphorus atom (Figure S2b) using either the single wavelength 1.2Å dataset or the remote wavelength of the SeMet data set and protein model phases only (not including cofactor or ligand). In both maps, the difference density contoured at 3σ shows electron density surrounding only those atoms with a significant anomalous signal at the wavelength of data collection (namely P, Mg^{2+}, and Se or S).

The *B*-factors of the liganded intermediate are similar to those of the surrounding atoms. The tensors that define the atomic motions can be visualized directly from the anisotropic B-factors (Figure S4). For the β-G1,6-P intermediate and the surrounding protein side-chains the tensors that define the atomic motions are symmetrical and fairly tight around the atom center. This result is consistent with the low *B*-factors for the covalent intermediate and liganding active-site residues.

The phosphorylated enzyme-Mg(II) complex assumes a conformation that leaves the active site accessible to bulk solvent (*3*). In contrast, calculation of the Connolly surface of the enzyme Mg(II)-β-G1,6-P complex demonstrates that the active site is solvent inaccessible. This is accomplished by the rigid motion of the "cap" domain (residues 16-78) relative to the "core" domain along an effective hinge axis by 25.7° as calculated by the program DynDom (*14*). The movement of the cap domain brings residues R49 and K76 within distance to form hydrogen bonds (directly or through water) to the C(6) phosphorus of G1,6-P (see Figure S3). In contrast to the large motions of the cap domain, numerous subtle changes in the orientation of the core domain residues which lead to shorter hydrogen bonds to the C(1) phosphorus of β-G1,6-P compared to the interactions with the aspartylphosphate phosphorus in the enzyme-Mg(II) complex.
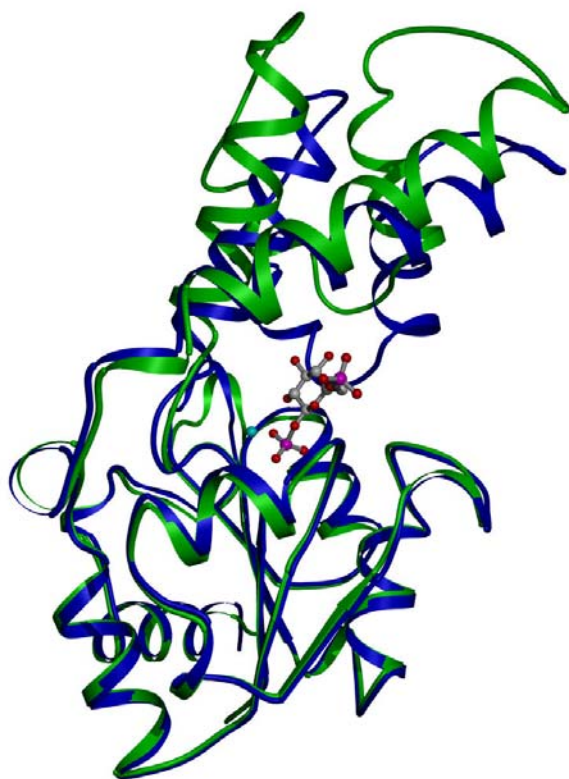
Figure S1: Overlay of the β-G1,6-P intermediate complex (blue) with the phosphorylated enzyme-Mg(II) complex (green) shows the rigid-body movement associated with a catalytic cycle. The interdomain active site is marked by the β-G1,6-P intermediate (ball-and stick model).
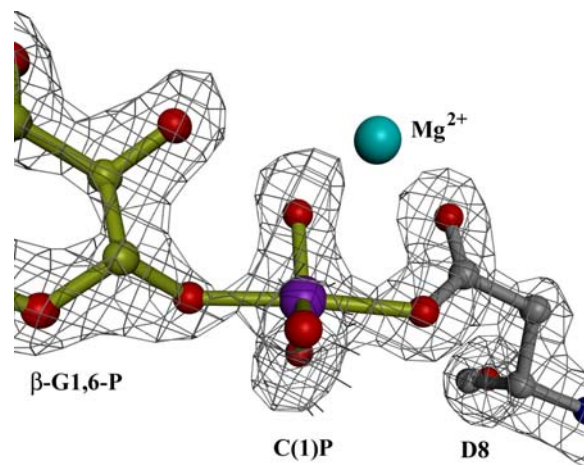
Figure S2a. The β-G1,6-P intermediate in the active site of β-PGM. The 1.2Å dataset was utilized to calculate a map to 2.0Å resolution (grey cages). The enzyme residues (gray) and β-G1,6-P intermediate (yellow) are shown as ball-and-stick with the Fo-Fc electron-density map contoured at 2σ (refined with simulated annealing and model omitted to remove bias).
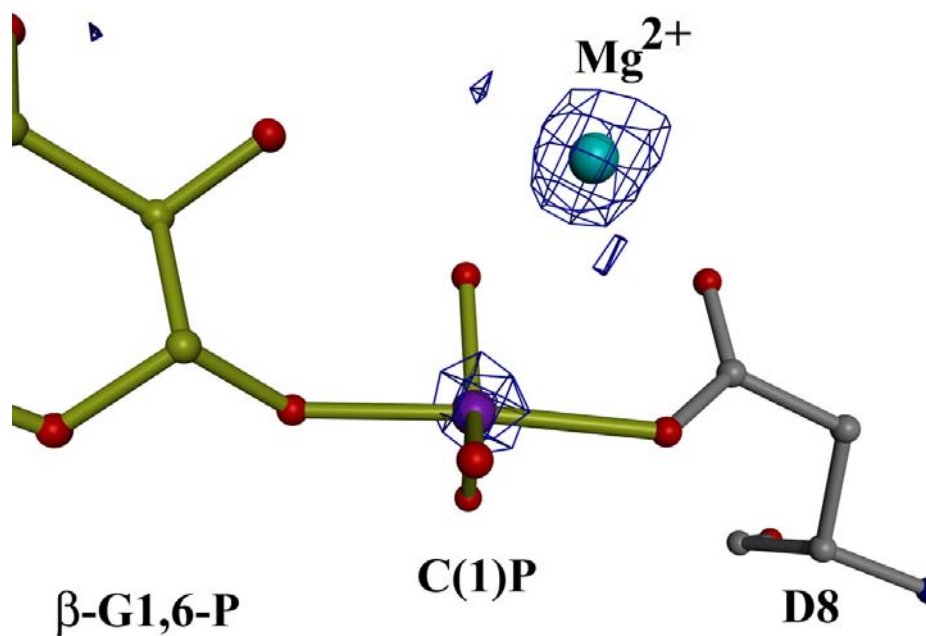
Figure S2b. The β-G1,6-P intermediate in the active site of β-PGM. The 1.2Å dataset was utilized to calculate an anomalous difference electron density map (countoured at 3σ, grey cages) using phases calculated from the protein model only (Mg^{2+} and ligand omitted). The enzyme residues (gray) and β-G1,6-P intermediate (yellow) are shown as ball-and-stick.
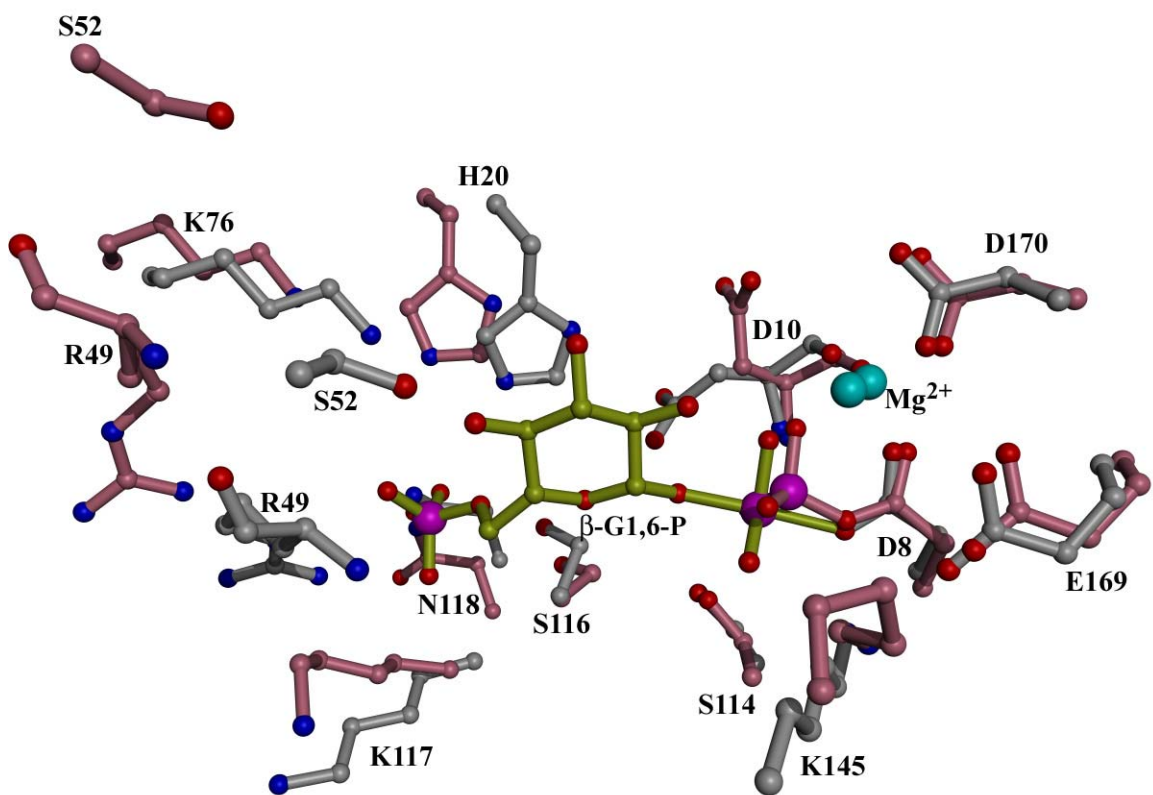
Figure S3. Overlay of the open (pink backbone) and the closed (light gray backbone) β-PGM active site.
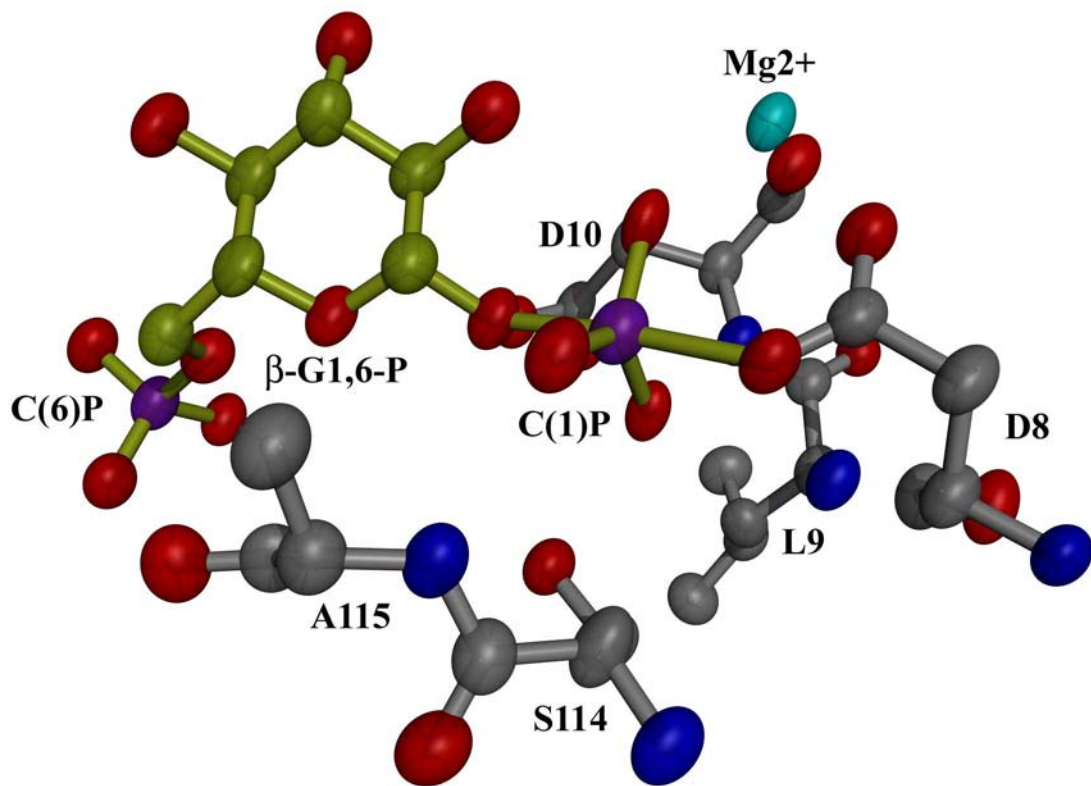
Figure S4. ORTEP diagram of the β-G1,6-P intermediate in the active site of β-PGM. The enzyme residues (gray) and β-G1,6-P intermediate (yellow) are shown as ball-and-stick.

Table S1. Individual Temperature Factors of the β-G1,6-P Intermediate

Atom[*]	Isotropic *B*-factor	
	G1P data set	G6P data set
C1	9.4	7.2
C2	9.8	8.0
O1	8.8	9.9
O5	8.7	8.9
C3	9.7	7.9
O2	8.9	8.5
C4	9.6	9.2
O3	10.2	9.1
C5	9.0	7.9
O4	10.6	10.3
C6	9.1	10.2
O6	9.3	8.8
PA	9.3	9.6
O1P	10.1	8.6
O2P	9.4	9.0
O3P	10.2	10.0
PB	9.4	7.9
O4P	9.9	12.7
O5P	8.5	16.0
O6P	8.0	9.1

[*]The atom names here are those given in the PDB file. In the text PA is called C(6)P and PB is called C(1)P.

References:

S1.   N. Qian, G. A. Stanley, B. Hahn-Hagerdal, P. Radstrom, *J. Bacteriol.* **176**, 5304 (1994).

S2.   N. Qian, G. A. Stanley, A. Bunte, P. Radstrom, *Microbiology* **143 (Pt 3)**, 855 (1997).

S3.   S. D. Lahiri, G. Zhang, D. Dunaway-Mariano, K. N. Allen, *Biochemistry* **41**, 8351 (2002).

S4.   Z. Otwinowski, W. Minor, *Methods Enzymol.* **276**, 307 (1997).

S5.   T. C. Terwilliger, J. Berendzen, *Acta Crystallogr. D Biol. Crystallogr.* **55 (Pt 4)**, 849 (1999).

S6.   T. C. Terwilliger, *Acta Crystallogr. D Biol. Crystallogr.* **55**, 1863 (1999).

S7.   T. A. Jones, J. Y. Zou, S. W. Cowan, Kjeldgaard, *Acta Crystallogr. A* **47 (Pt 2)**, 110 (1991).

S8.   A. T. Brünger *et al.*, *Acta Crystallogr. D Biol. Crystallogr.* **54 (Pt 5)**, 905 (1998).

S9.   R. J. Read, *Acta Cryst.* **A42**, 140 (1986).

S10.   T. Hisano *et al.*, *J. Biol. Chem.* **271**, 20322 (1996).

S11.   M. C. Morais *et al.*, *Biochemistry* **39**, 10385 (2000).

S12.   W. Wang, R. Kim, J. Jancarik, H. Yokota, S. H. Kim, *Structure* **9**, 65 (2001).

S13.   A. Rinaldo-Matthis, C. Rampazzo, P. Reichard, V. Bianchi, P. Nordlund, *Nat. Struct. Biol.* **10**, 779 (2002).

S14.   S. Hayward, A. Kitao, H. J. Berendsen, *Proteins* **27**, 425 (1997).